1 **Karst aquifer discharge response to rainfall interpreted as anomalous transport**

2 Dan Elhanati[1], Nadine Goeppert[2, 3], Brian Berkowitz[1]

3

4 [1]Department of Earth and Planetary Sciences, Weizmann Institute of Science, Rehovot, Israel

5 [2]Institute of Applied Geosciences, Division of Hydrogeology, Karlsruhe Institute of

6 Technology (KIT), Karlsruhe, Germany

7 [3]Institute of Geological Sciences, Hydrogeology, Free University Berlin, Germany

8

9 Correspondence to: Dan Elhanati (dan.elhanati@gmail.com)

10

11

12

13 **Abstract**

14 The discharge measured in karst springs is known to exhibit distinctive long tails during

15 recession times following distinct discharge peaks of short duration. The long-tail behavior is

16 generally attributed to the occurrence of tortuous, ramified flow paths that develop in the

17 underground structure of karst systems. Modeling the discharge behavior poses unique

18 difficulties because of the poorly-delineated flow path geometry and generally scarce

19 information on the hydraulic properties of catchment-scale systems. In a different context,

20 modeling of long-tailed behavior has been addressed in studies of chemical transport. Here, an

21 adaptation of a continuous time random walk – particle tracking (CTRW-PT) framework for

22 anomalous transport is proposed, which offers a robust means to quantify long-tailed

23 breakthrough curves that often arise during chemical species transport under various flow

24 scenarios. A theoretical analogy is first established between partially water-saturated karst flow,

25 characterized by temporally varying water storage, and chemical transport involving

26 accumulation and release of a chemical tracer. This analogy is then used to develop and

27 implement a CTRW-PT model. Application of this numerical model to examination of three

28 years of summer rainfall and discharge data from a karst aquifer system – the Disnergschroef

29 high alpine site in the Austrian Alps – is shown to yield robust fits between modeled and

30 measured discharge values. In particular, the analysis underscores the predominance of slow

31 diffusive flow over rapid conduit flow. The study affirms the analogy between partially

32 saturated karst flow and chemical transport, exemplifying the compatibility of the CTRW-PT

33 model for this purpose. Within the specific context of the Disnergschroef karst system, these

34 findings highlight the predominance of slow diffusive flow over rapid conduit flow. The

35 agreement between measured and simulated data supports the proposed analogy between

36 partially saturated karst flow and chemical transport; it also highlights the potential ability of

37 the anomalous transport framework to further enhance modeling of flow and transport in karst

38 systems.

1 Introduction

Aquifers consist of various geological formations through which water can flow and carry chemical species. The abundance of structural heterogeneities, ranging from intricate grain arrangements at the pore scale to larger geologic structures and discontinuities at the meso- and macroscopic scales, introduces irregular and tortuous flow paths that cannot be delineated without a full physical description of the system. Achieving an accurate representation of flow and transport therefore becomes increasingly difficult with an increase in the scale and complexity of the groundwater system.

Karst systems, in particular, are known as structurally complex aquifers. They are composed of many interconnected conduits, fractures and voids formed through the dissolution of soluble rocks like limestone, dolostone and gypsum, which leads to the occurrence of multiple and ramified flow paths (Bakalowicz, 2005). Karst terrains are usually described, in a vertical cross-section, by distinct hydrological layers whose structure affect the response of the system to incoming precipitation: (1) the surface soil layer; (2) the interface between the soil layer and the deeper saturated zone (epikarst); and (3) the deep underground, mostly phreatic, zone (endokarst). The soil and epikarst layers, known collectively as the exokarst, are known to exhibit lateral flow of water above and below ground, until water reaches fractures or conduits that allow them to flow rapidly to the endokarst. This allows for some water to infiltrate downwards, while some may remain in the vadose zone and be subjected to both percolation and evapotranspiration (Jukić and Denić-Jukić, 2009). The epikarst and endokarst layers each consist of a primary (matrix) porosity composed of all bulk pores, a secondary porosity composed of the smaller joints and fissure developed during diagenesis and/or by tectonic processes, and a tertiary porosity of large fractures and voids (conduits) created due to karstification (Ford and Williams, 2007). The different types of porosities usually exhibit distinct flow patterns: rapid flow in the conduits and slow diffusive flow in the smaller fissures and the matrix. The different karst layers may exhibit a changing role in facilitating the flow or retention of water through the system as a function of water level or recharge intensity (Hartmann et al., 2014).

To date, various hydrological models have been developed specifically for karst systems, to describe the commonly observed flow and transport patterns that are specific to karst systems. In particular, distributed models rely on creating a grid of cells with different hydrological parameters (e.g., Anderson & Radić, 2022; Chen et al., 2017; Kaufmann & Turk, 2016), while

71   lumped parameter models parameterize the characteristics of the system. Lumped parameter

72   models are based on different system conceptualizations (e.g., Chen and Goldscheider, 2014;

73   Cinkus et al., 2023b; Fleury et al., 2009; Jukić and Denić-Jukić, 2009; Mazzilli et al., 2019;

74   Rimmer and Salingar, 2006; Tritz et al., 2011), as well as neural network approaches (e.g.,

75   Afzaal et al., 2020; Cinkus et al., 2023b; Kratzert et al., 2018; Renard and Bertrand, 2017;

76   Wunsch et al., 2022). A common, significant feature encountered in karst systems – which is

77   difficult to capture in models – is the interplay of rapid and slow flow which manifests as long-

78   tailed measurements of both discharge rates (e.g., Frank et al., 2021) and chemical tracer

79   concentrations (e.g., Goeppert et al., 2020) observed at karst springs.

80   In many systems that exhibit highly variable spatial velocity distributions or temporal

81   behaviors, measurements of long tails in arrival times may be encountered. In the context of

82   chemical transport in porous media, long tails in the arrival time of chemical tracers have long

83   been a subject of study. Anomalous transport, which describes chemical transport that deviates

84   from the behavior described by the traditional Advection-Dispersion Equation (ADE), is

85   prevalent in many system and transport scenarios (Berkowitz et al., 2006); deviations from

86   solutions of traditional transport equations were observed even for non-dispersive diffusion

87   (Cortis and Knudby, 2006). It has been shown that higher subsurface heterogeneity increases

88   the degree of anomalous transport by inducing longer than expected (for Fickian transport)

89   arrival times (Edery et al., 2016, 2014). Traditional ADE based models, which rely on

90   averaging the physical traits of the medium into a single coefficient, do not accurately predict

91   transport in many cases. To correctly describe long-tailed events, various modeling approaches

92   have been developed. Among these, the Continuous Time Random Walk (CTRW) framework

93   has emerged as suitable for simulating diverse transport scenarios, including the behavior of a

94   long-time field-scale hydrological catchment (Dentz et al., 2023). The CTRW framework

95   accounts for anomalous transport behavior and offers a more physically realistic representation

96   of the transport processes that are encountered in real-world groundwater systems. The

97   framework defines waiting time and step length distributions that are applied in random walks

98   which are continuous in time, thereby capturing the complexity of transport processes

99   (Berkowitz et al., 2006).

100   In the current study, the CTRW framework, which has been developed to model anomalous

101   chemical transport, is utilized to quantify long-tailing of water flow in karst systems. In this

102   context, data from the Disnergschroef alpine study site in Vorarlberg, Austria are revisited

103   (Frank et al., 2021). This high-alpine karst system has been thoroughly studied and offers a

104 well-defined spatial catchment. The known extent of its recharge basin and the corresponding

105 single spring which serves as its outlet allow for measurements of both recharge and discharge.

106 Previous studies (e.g., Frank et al., 2021) identified a distinct discharge response approximately

107 5.5 hours after a rainfall event, with variations in electrical conductivity, indicative of fresh

108 rainfall arriving at the spring outlet, observed ~8 hours post-event. While existing models

109 provided a good overall fit and illuminated the divide between epikarst-to-conduit and matrix-

110 to-conduit flows, they were less effective in matching the long tails.

111 Accurate modeling of water movement in these complex subsurface landscapes is crucial, as

112 many regions rely on karst systems for drinking water (Stevanović, 2019). Here, a theoretical

113 and practical development of the CTRW framework is proposed as an approach to simulate the

114 intricate dynamics of water movement in karst environments.

115 **2 Conceptual and mathematical development**

116 The conceptual development of the CTRW framework to model water flow in karst systems is

117 founded on a proposed ansatz in which water flow is conceptualized as distinct "water parcels"

118 that travel along the available flow paths. Local volumes along the flow paths, e.g., caverns,

119 conduits, and voids, allow for the accumulation and release of water parcels, and define mobile

120 and immobile zones for water flow. The ansatz asserts that the accumulation and release of

121 water parcels in the various volumes in the karst system resemble the accumulation and release

122 of a chemical tracer over time in a porous medium. As shown in Fig. 1, a cavern acting as a

123 storage region for water parcels is analogous to tracer parcels accumulating in an immobile (or

124 less mobile) zone. For both cases, it should be noted that local accumulation of water parcels

125 or increase in concentration of a chemical will increase their respective fluxes in the immediate

126 local vicinity. Under similar hydraulic conditions both fluxes create distinctive long tails when

127 measured over a control plane at the system outlet, which is primarily a result of the structural

128 heterogeneity of the system.

129 Characterizing the flow of water through an infinitesimal control volume can be formulated in

130 terms of a balance equation that equates the net rate of fluid flow in the control volume to the

131 time rate of change of fluid mass storage within it:

132
$$-\frac{\partial(\rho q_x)}{\partial x} - \frac{\partial(\rho q_y)}{\partial y} - \frac{\partial(\rho q_z)}{\partial z} = \frac{\partial(\rho n)}{\partial t} \tag{1}$$

133 where n is porosity, ρ water density, and the three components of the specific discharge q are

134 described as q_x, q_y and q_z. This equation describes the mass balance in a fully saturated domain,

135   in which the void volume (V_v) is completely filled with water ($V_w=V_v$). The moisture content

136   ($\theta = \frac{V_w}{V_{tot}}$) in these cases is equal to the porosity, and the degree of saturation ($\theta' = \frac{\theta}{n}$) is equal

137   to 1.

138   For partially saturated flow, the degree of saturation is less than 1 and the moisture content is

139   smaller than n (as $V_w<V_v$). Adjusting the equation for partially saturated transient flow yields:

140
$$-\frac{\partial(\rho q_x)}{\partial x} - \frac{\partial(\rho q_y)}{\partial y} - \frac{\partial(\rho q_z)}{\partial z} = \frac{\partial(\rho \theta' n)}{\partial t} \quad . \tag{2}$$

141   Substituting $\theta' = \frac{\theta}{n}$:

142
$$-\frac{\partial(\rho q_x)}{\partial x} - \frac{\partial(\rho q_y)}{\partial y} - \frac{\partial(\rho q_z)}{\partial z} = \frac{\partial(\rho \theta)}{\partial t} \quad . \tag{3}$$

143   Deriving a description for a chemical tracer transport in a similar control volume is achieved

144   by a mass balance equation:

145
$$-\frac{\partial F_x}{\partial x} - \frac{\partial F_y}{\partial y} - \frac{\partial F_z}{\partial z} = n \frac{\partial C}{\partial t} \quad . \tag{4}$$

146   The chemical mass flux (in one direction) is defined by advection and diffusion terms:

147
$$F_i = q_i C - n D_i \frac{\partial C}{\partial i} \quad . \tag{5}$$

148   Substituting (5) into (4) yields

149
$$\frac{\partial}{\partial x}\left(n D_x \frac{\partial C}{\partial x}\right) - \frac{\partial}{\partial x}(q_x C) + \frac{\partial}{\partial y}\left(n D_y \frac{\partial C}{\partial y}\right) - \frac{\partial}{\partial y}(q_y C) + \frac{\partial}{\partial z}\left(n D_z \frac{\partial C}{\partial z}\right) - \frac{\partial}{\partial z}(q_z C) = n \frac{\partial C}{\partial t} \quad . \tag{6}$$

150   By drawing the analogy in the ansatz between the dynamics of water parcels and chemical

151   tracers, and noting the similar forms of Eqs. (3) and (4), the description of the mass balance of

152   water in a partially saturated domain is (at least) mathematically analogous to the description

153   of the mass balance of a chemical tracer in a saturated domain. This results in the intrinsic

154   connection of $C \Leftrightarrow \rho\theta$. In a 1D direction, the analogy of the mass flux can be thus defined:

155    $\rho q_x \equiv n D_x \frac{\partial C}{\partial x} - q_x C$. This connection incorporates hydrodynamic dispersion, which is

156   inherent in chemical transport resulting in observed long tails, into the description of the

157   partially saturated water parcels moving within the conceptual karst domain. Thus, the analogy

158   of chemical transport and water flow is expected to show long tailing in simple flow scenarios,

159   and was established even for pure diffusion (Cortis and Knudby, 2006).

160

161
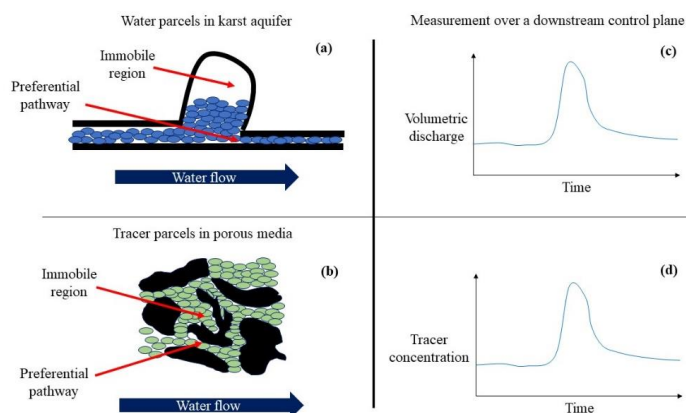
Figure 1. *Schematic illustration of (a) water parcels (blue ovals) in a karst aquifer; and (b) chemical tracer parcels (green ovals) in porous media (black grains) flowing through preferential pathways and accumulating in adjunct immobile regions. The resulting (schematic) measurements of the (c) temporal volumetric discharge and (d) tracer concentration that are measured at the spring outlet further downstream.*

167

Thus, transport equations – either advection-dispersion equations (ADE; Eq. (6)) for Fickian transport, or a CTRW formulation for non-Fickian transport (see Sect. 3.1) can be used, where the chemical tracer concentrations that these equations solve for $C(x,t)$ are conceptually identical to the relative concentration of water parcels. The concentration at a specific point is translated to a volume of water, so that a classical breakthrough curve $C(t)$ is reinterpreted as the (volumetric) amount of water per time reaching the domain outlet (or measurement plane).

3 Methods

3.1 CTRW-PT simulations

In this study, a particle tracking (PT) implementation of the CTRW framework was employed to devise a model capable of simulating spring discharge using the rainfall data as input. The CTRW-PT model, characterized by stochastically defined particle transitions, is a Lagrangian approach to solving the partial differential equations defined in the CTRW mathematical framework. The movement of the particles, representing water parcels as described in the ansatz (see Sect. 2), is described by equations that define the probability of particles to make

182   transitions in both space and time (Elhanati et al., 2023). For 1D cases, the transport is governed

183   by two probability density functions, $p(s)$ and $\psi(t)$, which define the particle movement in space

184   and time, respectively. An exponential from for $p(s)$ and a truncated power law (TPL) form for

185    $\psi(t)$ are used:

186
$$p(s) = \lambda_s^2 \exp(-\lambda_s s) \,, \tag{7}$$

187
$$\psi(t) = C \frac{\exp(-t/t_2)}{(1+t/t_1)^{1+\beta}} \,. \tag{8}$$

188   Here, λ_s^2 and C serve as normalization factors for $p(s)$ and $\psi(t)$, respectively. The TPL is

189   governed by β, the power law exponent ($0 < \beta < 2$), which is a measure of the non-Fickian

190   nature of the transport, t_1, the characteristic transition time, and t_2, the cutoff time to initiate

191   transition to Fickian transport. The particle velocity, v_ψ, and the generalized dispersion, D_ψ,

192   are defined as the first and second spatial moments of the chemical species plume in the flow

193   direction (Berkowitz et al., 2006) For a 1D system:

194
$$v_\psi = \frac{\overline{s_x}}{\bar{t}} = \frac{\int_0^\infty p(s)s^2 ds}{\int_0^\infty \psi(t)t dt} \,, \tag{9}$$

195
$$D_\psi = \frac{1}{2}\frac{\overline{s_x^2}}{\bar{t}} = \frac{1}{2}\frac{\int_0^\infty p(s)s^3 ds}{\int_0^\infty \psi(t)t dt} \,, \tag{10}$$

196   where $\overline{s_x}$ and $\bar{t}$ are the mean step size and time, respectively.

197   Inserting the probability density functions (Eqs. 7 and 8) into Eqs. 9 and 10, and defining $\tau_2 \equiv$

198   t_2/t_1 yields a mathematical relation among v_ψ, D_ψ, β, τ_2, t_1, t_2 and λ_s (see Nissan et al., 2017

199   for a full mathematical development). By treating the first four variables (v_ψ, D_ψ, β, τ_2) as

200   fitting parameters, the other three (t_1, t_2, λ_s) are immediately determined, allowing

201   optimization of the CTRW-PT model to a specific flow scenario (see Table 1).

202   The intricate three-dimensional flow field of a karst system can be conceptualized in a model

203   that considers the relationships between storage and discharge. These kinds of models, known

204   as lumped models, have been extensively used in simulation of karst systems (Hartmann et al.,

205   2014). Herein, a similar approach is applied, i.e., conceptualizing the system as a series of

206   specific physical transitions. However, in the context of the CTRW-PT model, an equivalent

207   medium to the karst system is defined in the form of a one-dimensional domain. Water is

208   introduced into the domain along its entire extent and flows to the domain outlet.

209　The 1D conceptualization is facilitated by the well-defined spatial characteristics of the system,

210　namely the catchment area and spring outlet (Fig. 2a). The distance of each point on the surface

211　of the catchment to the spring outlet is calculated (Fig. 2b), which yields a distances frequency

212　histogram (Fig. 3). A normal distribution, fitted to the histogram using MATLAB, dictates how

213　new particles are introduced into the system along the 1D domain (physically unrealistic,

214　negative sampled values are set to 0). The actual underground flow path between each point

215　and the outlet spring is longer than the linear distance between the two points, as the water

216　must travel through the tortuous path through the existing conduits and fissures. The distances

217　are therefore multiplied by an empirical tortuosity factor (L), which serves as an optimization

218　parameter (see Table 1).
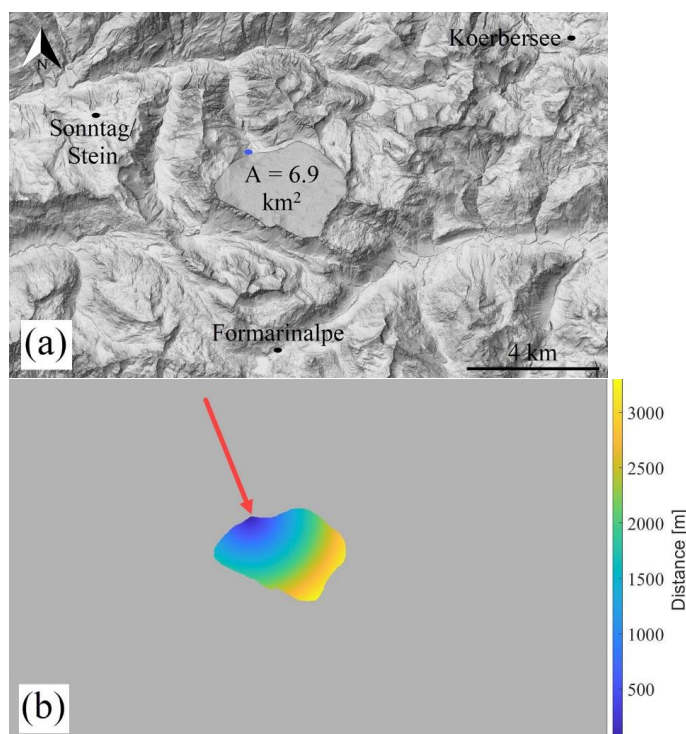
220　**Figure 2.** (a) *Map of the Disnergschroef study area. The three weather stations in which rainfall*

221　*was measured are marked with black dots, the measured spring outlet is marked with a blue*

222　*dot (basemap: Land Vorarlberg – data.vorarlberg.gv.at); (b) Distances from the catchment*

223　*area to the spring outlet. The distances are marked by a color scale. The spring outlet is marked*

224　*by a red arrow.*

Hydrology and
Earth System
Sciences
Discussions

Open Access
EGU

225


226
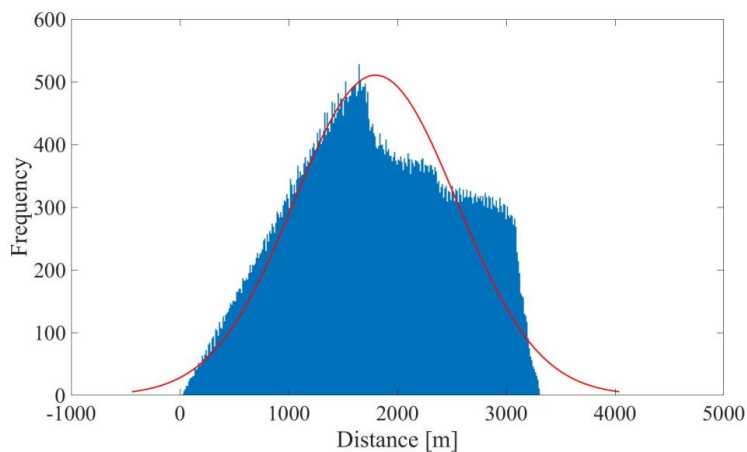
Figure 3. *Distribution of distances from catchment area to spring outlet. The red line represents a fitted normal distribution ($\mu=1.8\times10^3$; $\sigma=747$).*

Discharge at the spring is sampled every 15 minutes ($L\,s^{-1}$). The discharge minimum represents baseflow conditions. Raw rainfall data from three nearby weather stations (Fig. 2a) are measured in millimeters per 15 minutes. The data from the three stations are averaged, and the catchment area is used to convert the data into liters per second (Fig. 4). To achieve higher temporal simulation resolution, linear interpolation was used to resample the time series to match a smaller simulation time step (100 s).

235
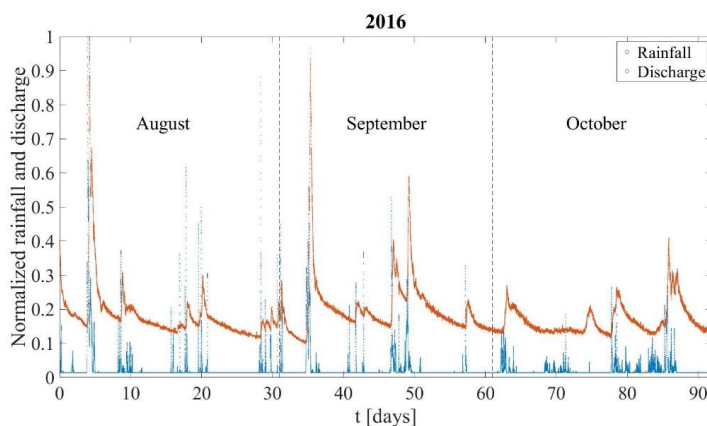
236
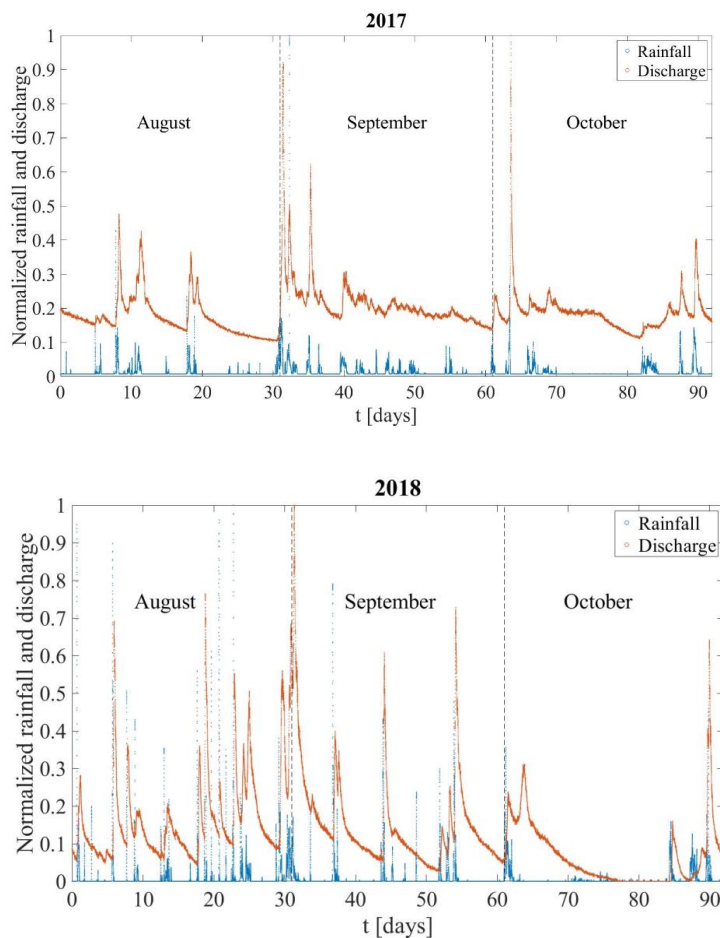
237

238 **Figure 4.** *Rainfall and discharge curves for the 2016, 2017 and 2018 datasets. The data are*

239 *normalized according to the maximum rainfall and discharge values, respectively, for each of*

240 *the three years.*

241

242 For an ideal system, in which all incoming rainwater is discharged through the spring outlet,

243 the ratio of total rainwater to total discharge is expected to be unity. However, considering the

244 uncertainty in the contributions of hydraulic parameters to the catchment water budget, e.g.,

245 flow to deeper parts of the aquifer and/or other springs, and evapotranspiration, the rainfall

246 function must be adjusted by a calculated observed recharge capacity to yield the recharge
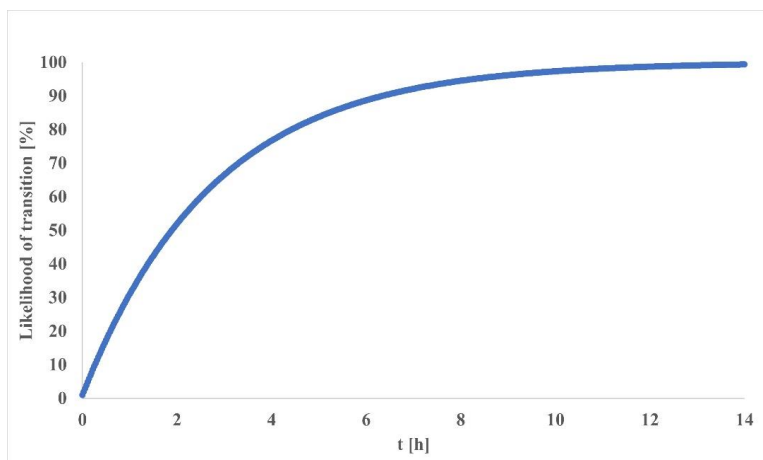
247 function:

248 $$recharge(t) = rainfall(t) \times \frac{\sum discharge(t) - baseflow}{\sum rainfall(t)} \qquad (11)$$

11

249 where *rainfall*(*t*) and *discharge*(*t*) are the measured rainfall and discharge time series. The ratio

250 multiplying the rainfall function is defined here as the recharge capacity parameter. The

251 baseflow was subtracted from the total discharge for the recharge capacity calculation, to

252 account for the background discharge not related to the spring response to rainfall.

253 A common procedure in lumped karst models separates the flow into slow and fast components,

254 representing the diffusive flow in the matrix and smaller fissures and the rapid flow in the

255 conduits, respectively (Hartmann et al., 2014). The CTRW-PT, as opposed to lumped models,

256 does not utilize water flow reservoirs, and operates by tracking the motion of particles that

257 represent water parcels. Therefore, the model was adapted to implement a similar approach:

258 two different sets of CTRW parameters, which govern the probability density functions for

259 particle movement (see Eqs. 7-10), are defined to represent the two flow regimes. Each particle

260 in the simulation is defined as "slow" or "fast", and therefore obeys the corresponding set of

261 CTRW parameters (see Table 1). Newly introduced particles are divided between fast and slow

262 flow, according to a set ratio (SF_r), and they advance in space and time by their corresponding

263 set of CTRW parameters. Furthermore, each slow particle has a likelihood to transition into a

264 fast particle (SF_l) in each simulation iteration, by changing the set of CTRW parameters that

265 the particle obeys. The transition from slow to fast flow illustrates the flow of water from the

266 matrix/fissures to the conduits.

267 As depicted in Fig. 5, the likelihood of particle transition increases rapidly, with slow particles

268 consistently transitioning into fast particles. For a transition likelihood of 0.01% and a

269 simulation time step of 100 s, the likelihood for a single particle to make a transition surpasses

270 99% after 458 steps which amount to 45,800 seconds (~12.7 hours). In comparison, the data

271 and simulations presented in this study span a duration of 7,951,400 seconds (~92 days). These

272 two parameters, governing the division of water between fast and slow flow and the transition

273 of water from the matrix/fissures to the conduits, are pivotal in allowing the CTRW-PT model

274 to simulate karst data.

Figure 5. *Likelihood of particle transition from slow regime to fast regime (SF_l) as a function time, representing a particle transition from slow matrix/fissure flow to fast conduit flow.*

3.2 Model optimization and comparison to field measurements

Each particle represents a volume of water. The volume per particle was calculated by dividing the total observed rainfall volume by the number of simulation particles. This enables a comparison between simulated and observed recharge by volume. Given the presence of numerous model parameters (refer to Table 1), optimization is achieved by minimizing the Root Mean Squared Error (RMSE) between observed and simulated discharge using different combinations of parameter values. The 2016 dataset was first utilized for parameter optimization, while the 2017 and 2018 datasets served as targets for validation, by considering them for prediction using the optimized parameters from the 2016 dataset.

The Nash-Sutcliffe efficiency (NSE) was calculated for the optimized simulations, as a measure of the goodness of fit. It is described as a normalized variant of the mean squared error:

$$NSE = 1 - \frac{\sum(x_s(t) - x_o(t))^2}{\sum(x_o(t) - \mu_o)^2} \tag{12}$$

where x_s is the simulated discharge, x_o is the observed discharge and μ_o is the observed mean. The NSE performance criterion is widely used in hydrological studies and does not induce counterbalancing errors (Cinkus et al., 2023a).

4 Results and Discussion

4.1 Optimized simulations of measured discharge

The optimized simulation for the 2016 dataset yields a fit (Fig. 6) that captures both the rapid response of the spring discharge to rainfall events and the protracted relaxation times characterized by the long tails evident after rainfall events. The optimized model parameters for the slow diffusive and fast conduit flow components are detailed in Table 1.

Table 1. *Optimized model parameters.*

Parameter	Optimized value	Description
v_ψ^f	360 m h^{-1}	Fast v_ψ
D_ψ^f	36 m^2 h^{-1}	Fast D_ψ
β^f	1.7	Fast β
τ_2^f	10^6	Fast τ_2
v_ψ^s	18 m h^{-1}	Slow v_ψ
D_ψ^s	3.6 x 10^8 m^2 h^{-1}	Slow D_ψ
β^s	1.2	Slow β
τ_2^s	10^8	Slow τ_2
L	1.6	Tortuosity
SF_r	0.95	Slow to fast particle ratio
SF_l	0.01 %	Slow to fast particle transition likelihood
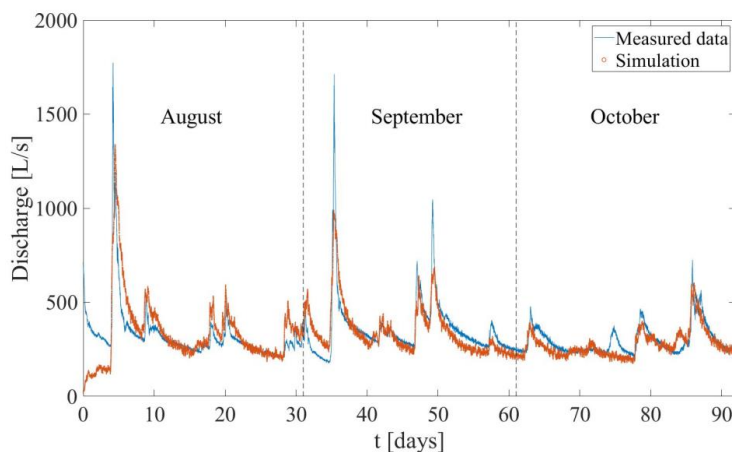
Figure 6. *Measured and simulated spring discharge for the 2016 dataset (NSE=0.5).*

Hydrology and
Earth System
Sciences
Discussions

Open Access

EGU

305   The differences between the fast and slow flow components, as illustrated by the respective

306   optimized CTRW parameters, elucidate the contribution of each flow component to the

307   volumetric discharge. The fast flow velocity parameter ($v_\psi^f = 360\ m\ h^{-1}$) is much larger than

308   the slow flow velocity parameter ($v_\psi^s = 18\ m\ h^{-1}$), and shows how incoming rain can rapidly

309   flow to the spring outlet, when travelling through the large conduits. The slow diffusive flow,

310   however, has a much longer travel time than the fast flow. Another clear difference between

311   the two components which is evident from the optimized values is the degree of anomalous

312   transport. The fast flow β (1.7) and τ_2 (10^6) parameters lead to a more symmetrical contribution

313   to the resulting discharge around the peak following the recharge event, compared to the slow

314   flow parameters (β=1.2, τ_2=10^8), which create a long tail after the discharge peak. The slow

315   flow is also much more dispersive ($D_\psi^s = 3.6\ x\ 10^8\ m^2\ h^{-1}$) compared to the fast flow ($D_\psi^f =$

316      $36\ m^2\ h^{-1}$), which contributes further to the long discharge tails. The optimized parameters

317   show a strong prominence of the slow flow over the fast flow: 95% of newly introduced

318   particles are introduced as slow particles (SF_r), with a 0.01% likelihood for a slow particle to

319   transition at each iteration to a fast regime (SF_l).

320   The fit obtained for the 2016 dataset modeling is satisfactory considering the inherent

321   uncertainty associated with the input data. The three weather stations used to measure the

322   precipitation are not located inside the catchment area, and different precipitation data were

323   measured at each station, which can be seen by examining the cross-correlation coefficients

324   between the 2016 discharge and rainfall data: 0.20, 0.22 and 0.15 for stations Koerbersee,

325   Formarinalpe, Sonntag/Stein, respectively (Fig. 2a). While an average of the three stations

326   provides an acceptable estimate of the recharge over the given time period, the variability of

327   local rain events is overlooked, which may be common in the high mountainous topography.

328   This is especially true in extreme rain events, in which variations of onset, duration, and total

329   discharge of an event can induce different responses of the modeled discharge.

330   The same set of CTRW parameters optimized for the 2016 data – without further adjustment –

331   was employed to interpret the 2017 and 2018 datasets (Fig. 7). Both datasets show that the

332   simulated discharge after rainfall events predicts the onset, length and volume of the measured

333   discharge. This is especially true for the many discharge peaks exhibited by the 2018 data.
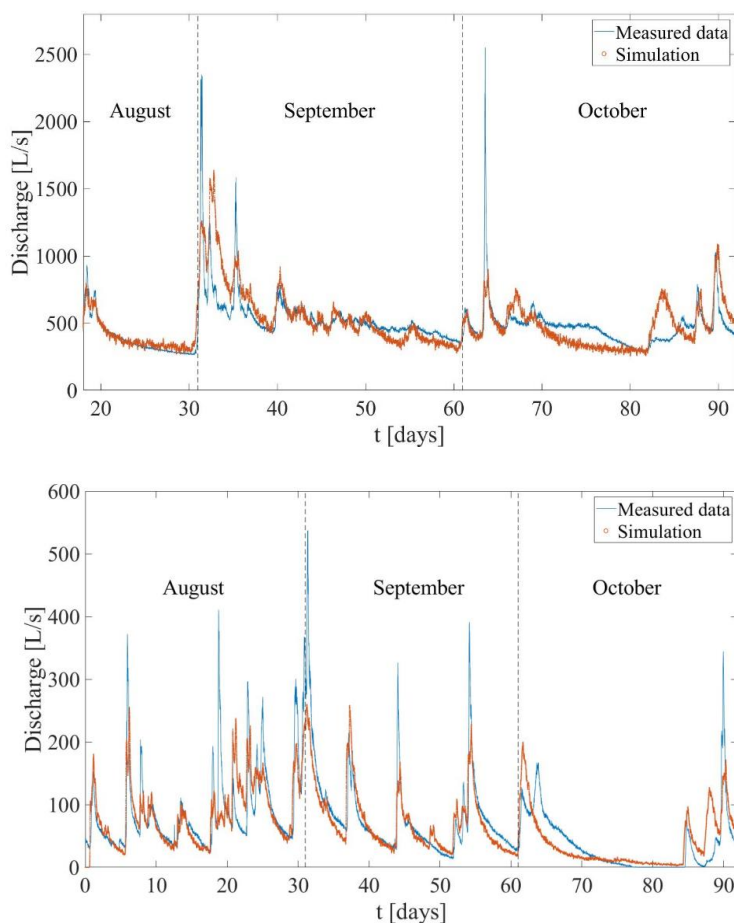
Figure 7. *Measured and simulated spring discharge for the 2017 (top; NSE=0.33) and 2018 (bottom; NSE=0.63) datasets. Note that due to the large differences in maximum discharge between the three years, the vertical scales in Fig. 6 and in Fig. 7 are adjusted accordingly.*

The recharge capacity parameter (applied to calculate the recharge function from the measured rainwater; see Eq. 11) was calculated as 0.43 and 0.45 for the 2016 and 2017 datasets, respectively. These values suggest that ~40% of the incoming rainfall reaches the outlet spring, with the remaining water reaching deeper parts of the aquifer that are less mobile. The drier 2018 dataset, however, displayed a much lower value of 0.19. The variability of the recharge capacity parameter in different time periods, as a function of the rainfall pattern and amount,

345 highlights the importance of this parameter to the correct prediction of the system discharge
346 response to rainfall.

4.2 Prominence of the slow flow component in the Disnergschroef system

348 The prominence of the slow component in this karst system is evident from both the high SF_r
349 and low SF_l. The consistency of this finding, across the three datasets (Fig. 6 and 7), agrees
350 with the analysis by Frank et al. (2021) of the recharge/discharge relationship. They observed
351 that while the flow from epikarst to conduit and matrix is highly variable and rainfall-
352 dependent, the matrix to conduit flow remains relatively constant up to a threshold. The
353 coupling of the two flow processes produces a distinctive discharge pattern characterized by a
354 sharp rapid peak after a rainfall event, followed by a long tail during recession and a return to
355 baseflow. The current analysis is similar and further emphasizes that the volumetric
356 contribution of the slow flow is substantial, particularly influencing the extended tails. In
357 contrast, the fast flow plays a more straightforward role, contributing predominantly to
358 discharge peaks by quickly expelling introduced rainwater from the system.

359 Given the importance of karst systems for human consumption, monitoring and prediction of
360 system discharge is especially important during high and low flow scenarios. These extreme
361 events can have consequences on water quality, including over-consumption during dry periods
362 and increases in turbidity and bacterial activity in high flow conditions (Pronk et al., 2006).
363 The frequency of both dry periods and heavy rainfall events has been shown to rise due to
364 climate change (Stoll et al., 2011), and this may well increase in the near future. In this context,
365 the high peaks and long tails associated with these flow conditions have proven to be the most
366 difficult to correctly predict, across different karst modeling approaches (Jeannin et al., 2021).
367 The results presented of the CTRW modeling exhibits the long tails associated with low water
368 flow. The 2018 dataset, in particular, which represents a dry summer compared to the other two
369 datasets, exemplifies the robustness of the model in predicting low flow conditions.

**4.3 The contribution of the slow and fast flow components to simulated discharge**

371 The results for all three datasets do not show agreement between the maximum simulated and
372 observed discharge values that are found immediately after high recharge events. The better fit
373 of the long tails compared to the high peaks is evident in the improvement of the NSE values
374 presented above (0.50, 0.33, 0.63 for 2016, 2017 and 2018, respectively), when calculated for
375 the data without the prominent peaks (0.75, 0.60, 0.65 for 2016, 2017 and 2018, respectively).
376 The dry 2018 dataset is the least affected from removing the peak for the NSE calculation

Hydrology and
Earth System
Sciences
Discussions
Open Access

EGU

377 because the peaks are low relatively to the 2016 and 2017 datasets. The fast response of

378 discharge to the incoming rain in karst systems after high recharge events has been described

379 in previous studies as a piston effect (Aquilina et al., 2006; Hartmann et al., 2014). Incoming

380 rain creates a rise in discharge before the rainwater reaches the outlet, as the increase in

381 hydraulic head pushes out water that was retained in the system before the rain. This effect was

382 shown specifically in the Disnergschroef system by Frank et el. (2021) which measured a 2.5-

383 hour difference between the first response of spring discharge to a rainfall event, to the arrival

384 of the rainwater to the outlet. The model herein does not take this effect into account, which

385 creates the negative bias in modeling the high peaks. While outside the scope of this study, this

386 can be addressed in the future by adding a third flow component, or by altering the CTRW

387 parameters of the particles present in the system prior to the rainfall event to represent the

388 increase in flow velocity.

389 To further examine the effect of both the slow and fast flow components on the simulated

390 discharge, simulations that examine the SF_l and SF_r parameters across a wider range were

391 conducted (Fig. 8). Simulations that contained only fast or slow particles (Fig. 8a), clearly show

392 that fast flow discharge responds very quickly to rainfall and produces no observable tails. In

393 contrast, the slow flow produces very long tails. It is noteworthy that the first response of the

394 slow flow is similar to the fast flow, as particles that are introduced to the system close to the

395 outlet have a very short length to travel to reach the outlet. Mixing of both flow regimes, either

396 by directly splitting the particles between the two regimes as they are introduced (Fig. 8b) or

397 by changing the transition likelihood (Fig. 8c) produces an intermediate response: as more of

398 the flow is slow, longer tails are found but the peaks are smaller.

399

Hydrology and
Earth System
Sciences
Discussions

Open Access

EGU
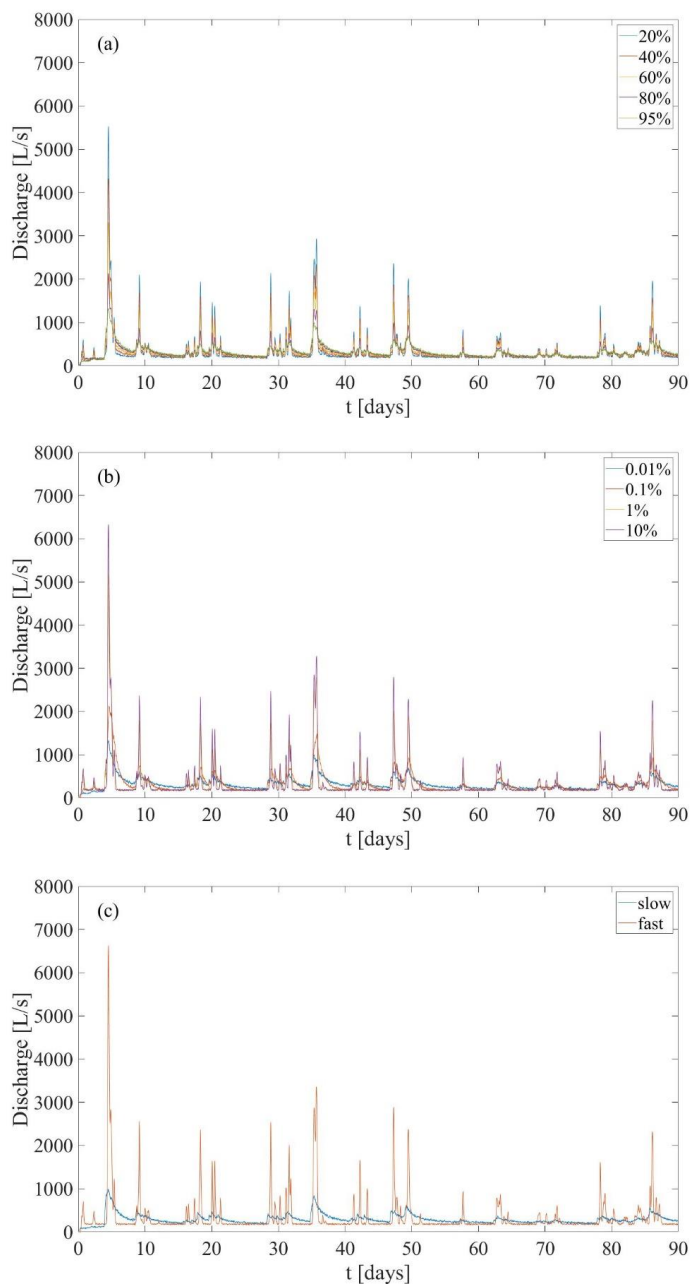
Figure 8. *Simulation sensitivity to slow and fast particle contribution, based on the 2016 rainfall data. Simulations containing only one kind of particle (a), Slow/Fast ratio (b) and transition likelihood from slow to fast (c) demonstrate the importance of the slow flow for the observed long tails in the discharge data.*

5 Conclusions

An analogy between partially saturated water flow in karst aquifers and anomalous chemical transport is established, allowing for the adaption of the CTRW-PT model to water flow in general, and for karst discharge response to rainfall specifically. The model was calibrated on one summer season of measurements of spring outlet discharge response to incoming rain; it was then used to predict the long tails observed in discharge measurements following rainfall events in two subsequent summer seasons.

The investigation of the Disnergschroef karst system has showed that slow diffusive flow is a predominant contributor to the volumetric discharge response to recharge events, in comparison to fast conduit flow. This finding highlights the nuanced interplay between fast and slow flow components in karst systems, and how they both evolve over time and as a function of the recharge intensity.

The theoretical and practical advancements presented here offer a potentially robust tool to further assess long-tailed rainfall-discharge responses in karst systems and other complex, catchment-scale systems.

Hydrology and
Earth System
Sciences
Discussions

Open Access

EGU

Data availability

The data on which this article is based are available online on Zenodo: https://zenodo.org/doi/10.5281/zenodo.10635639 (Elhanati and Berkowitz, 2024).

Author contribution

DE, NG and BB formulated the ideas which originated the project and defined the goals and aims of the study. DE developed and implemented the methodology and carried out the data analysis. DE and BB drafted the initial manuscript. All authors took part in reviewing and editing the final manuscript.

Competing interests

BB is a member of the editorial board of the journal.

Acknowledgments

References

Afzaal, H., Farooque, A. A., Abbas, F., Acharya, B., and Esau, T.: Groundwater estimation from major physical hydrology components using artificial neural networks and deep learning, Water (Switzerland), 12, https://doi.org/10.3390/w12010005, 2020.

Anderson, S. and Radić, V.: Evaluation and interpretation of convolutional long short-term memory networks for regional hydrological modelling, Hydrol. Earth Syst. Sci., 26, 795–825, https://doi.org/10.5194/hess-26-795-2022, 2022.

Aquilina, L., Ladouche, B., and Dörfliger, N.: Water storage and transfer in the epikarst of karstic systems during high flow periods, J. Hydrol., 327, 472–485, https://doi.org/10.1016/j.jhydrol.2005.11.054, 2006.

451 Bakalowicz, M.: Karst groundwater: A challenge for new resources, Hydrogeol. J., 13, 148–

452 160, https://doi.org/10.1007/s10040-004-0402-9, 2005.

453 Berkowitz, B., Cortis, A., Dentz, M., and Scher, H.: Modeling non-Fickian transport in

454 geological formations as a continuous time random walk, Rev. Geophys., 44, 1–49,

455 https://doi.org/10.1029/2005RG000178, 2006.

456 Chen, Z. and Goldscheider, N.: Modeling spatially and temporally varied hydraulic behavior

457 of a folded karst system with dominant conduit drainage at catchment scale, Hochifen-

458 Gottesacker, Alps, J. Hydrol., 514, 41–52, https://doi.org/10.1016/j.jhydrol.2014.04.005,

459 2014.

460 Chen, Z., Hartmann, A., and Goldscheider, N.: A new approach to evaluate spatiotemporal

461 dynamics of controlling parameters in distributed environmental models, Environ. Model.

462 Softw., 87, 1–16, https://doi.org/10.1016/j.envsoft.2016.10.005, 2017.

463 Cinkus, G., Mazzilli, N., Jourde, H., Wunsch, A., Liesch, T., Ravbar, N., Chen, Z., and

464 Goldscheider, N.: When best is the enemy of good - critical evaluation of performance

465 criteria in hydrological models, Hydrol. Earth Syst. Sci., 27, 2397–2411,

466 https://doi.org/10.5194/hess-27-2397-2023, 2023a.

467 Cinkus, G., Wunsch, A., Mazzilli, N., Liesch, T., Chen, Z., Ravbar, N., Doummar, J.,

468 Fernández-Ortega, J., Barberá, J. A., Andreo, B., Goldscheider, N., and Jourde, H.:

469 Comparison of artificial neural networks and reservoir models for simulating karst spring

470 discharge on five test sites in the Alpine and Mediterranean regions, Hydrol. Earth Syst. Sci.,

471 27, 1961–1985, https://doi.org/10.5194/hess-27-1961-2023, 2023b.

472 Cortis, A. and Knudby, C.: A continuous time random walk approach to transient flow in

473 heterogeneous porous media, Water Resour. Res., 42, 1–5,

474 https://doi.org/10.1029/2006WR005227, 2006.

475 Dentz, M., Kirchner, J. W., Zehe, E., and Berkowitz, B.: The role of anomalous transport in

476 long-term, stream water chemistry variability, Geophys. Res. Lett., 50, 1–8,

477 https://doi.org/10.1029/2023GL104207, 2023.

478 Edery, Y., Geiger, S., and Berkowitz, B.: Structural controls on anomalous transport in

479 fractured porous rock, Water Resour. Res., 52, 5634–5643, https://doi.org/10.1111/j.1752-

480 1688.1969.tb04897.x, 2016.

481 Edery, Y., Guadagnini, A., Scher, H., and Berkowitz, B.: Origins of anomalous transport in

482 heterogeneous media: Structural and dynamic controls, Water Resour. Res., 50, 1490–1505,

483 https://doi.org/10.1111/j.1752-1688.1969.tb04897.x, 2014.

484 Elhanati, D. and Berkowitz, B.: CTRW simulations of karst aquifer discharge response to

485 rainfall [Data Set], Zenodo, https://doi.org/10.5281/zenodo.10635640, 2024.

486 Elhanati, D., Dror, I., and Berkowitz, B.: Impact of time-dependent velocity fields on the

487 continuum-scale transport of conservative chemicals, Water Resour. Res., 59, 1–19,

488 https://doi.org/10.1029/2023WR035266, 2023.

489 Fleury, P., Ladouche, B., Conroux, Y., Jourde, H., and Dörfliger, N.: Modelling the

490 hydrologic functions of a karst aquifer under active water management - The Lez spring, J.

491 Hydrol., 365, 235–243, https://doi.org/10.1016/j.jhydrol.2008.11.037, 2009.

492 Ford, D. and Williams, P.: Karst Hydrogeology and Geomorphology, 1–562 pp.,

493 https://doi.org/10.1002/9781118684986, 2007.

494 Frank, S., Goeppert, N., and Goldscheider, N.: Improved understanding of dynamic water and

495 mass budgets of high-alpine karst systems obtained from studying a well-defined catchment

496 area, Hydrol. Process., 35, 1–15, https://doi.org/10.1002/hyp.14033, 2021.

497 Goeppert, N., Goldscheider, N., and Berkowitz, B.: Experimental and modeling evidence of

498 kilometer-scale anomalous tracer transport in an alpine karst aquifer, Water Res., 178,

499 115755, https://doi.org/10.1016/j.watres.2020.115755, 2020.

500 Hartmann, A., Goldscheider, N., Wagner, T., Lange, J., and Weiler, M.: Karst water resources

501 in a changing world: Review of hydrological modeling approaches, Rev. Geophys., 52, 218–

502 242, https://doi.org/10.1002/2013RG000443, 2014.

503 Jeannin, P. Y., Artigue, G., Butscher, C., Chang, Y., Charlier, J. B., Duran, L., Gill, L.,

504 Hartmann, A., Johannet, A., Jourde, H., Kavousi, A., Liesch, T., Liu, Y., Lüthi, M., Malard,

505 A., Mazzilli, N., Pardo-Igúzquiza, E., Thiéry, D., Reimann, T., Schuler, P., Wöhling, T., and

506 Wunsch, A.: Karst modelling challenge 1: Results of hydrological modelling, J. Hydrol., 600,

507 https://doi.org/10.1016/j.jhydrol.2021.126508, 2021.

508 Jukić, D. and Denić-Jukić, V.: Groundwater balance estimation in karst by using a conceptual

509 rainfall-runoff model, J. Hydrol., 373, 302–315,

510 https://doi.org/10.1016/j.jhydrol.2009.04.035, 2009.

511 Kaufmann, G. and Turk, J.: Modelling flow of subterranean Pivka river in Postojnska jama ,

512 Slovenia Modeliranje toka podzemeljske Pivke v Postojnski, 57–70, 2016.

513 Kratzert, F., Klotz, D., Brenner, C., Schulz, K., and Herrnegger, M.: Rainfall-runoff

514 modelling using Long Short-Term Memory (LSTM) networks, Hydrol. Earth Syst. Sci., 22,

515 6005–6022, https://doi.org/10.5194/hess-22-6005-2018, 2018.

516 Mazzilli, N., Guinot, V., Jourde, H., Lecoq, N., Labat, D., Arfib, B., Baudement, C.,

517 Danquigny, C., Dal Soglio, L., and Bertin, D.: KarstMod: A modelling platform for rainfall -

518 discharge analysis and modelling dedicated to karst systems, Environ. Model. Softw., 122,

519 https://doi.org/10.1016/j.envsoft.2017.03.015, 2019.

520 Nissan, A., Dror, I., and Berkowitz, B.: Time-dependent velocity-field controls on anomalous

521 chemical transport in porous media, Water Resour. Res., 53, 3760–3769,

522 https://doi.org/10.1111/j.1752-1688.1969.tb04897.x, 2017.

523 Pronk, M., Goldscheider, N., and Zopfi, J.: Dynamics and interaction of organic carbon,

524 turbidity and bacteria in a karst aquifer system, Hydrogeol. J., 14, 473–484,

525 https://doi.org/10.1007/s10040-005-0454-5, 2006.

526 Renard, P. and Bertrand, C.: EuroKarst 2016, Neuchâtel, Advances in the Hydrogeology of

527 Karst and Carbonate Reservoirs, 217–229 pp., 2017.

528 Rimmer, A. and Salingar, Y.: Modelling precipitation-streamflow processes in karst basin:

529 The case of the Jordan River sources, Israel, J. Hydrol., 331, 524–542,

530 https://doi.org/10.1016/j.jhydrol.2006.06.003, 2006.

531 Stevanović, Z.: Karst waters in potable water supply: a global scale overview, Environ. Earth

532 Sci., 78, 1–12, https://doi.org/10.1007/s12665-019-8670-9, 2019.

533 Stoll, S., Hendricks Franssen, H. J., Butts, M., and Kinzelbach, W.: Analysis of the impact of

534 climate change on groundwater related hydrological fluxes: A multi-model approach

535 including different downscaling methods, Hydrol. Earth Syst. Sci., 15, 21–38,

536 https://doi.org/10.5194/hess-15-21-2011, 2011.

537 Tritz, S., Guinot, V., and Jourde, H.: Modelling the behaviour of a karst system catchment

538 using non-linear hysteretic conceptual model, J. Hydrol., 397, 250–262,

539 https://doi.org/10.1016/j.jhydrol.2010.12.001, 2011.

540 Wunsch, A., Liesch, T., Cinkus, G., Ravbar, N., Chen, Z., Mazzilli, N., Jourde, H., and

541   Goldscheider, N.: Karst spring discharge modeling based on deep learning using spatially

542   distributed input data, Hydrol. Earth Syst. Sci., 26, 2405–2430, https://doi.org/10.5194/hess-

543   26-2405-2022, 2022.

544